Proceedings of the ASME 2015 International Design Engineering Technical Conferences & Computers and Information in Engineering Conference
IDETC/CIE 2015
August 2-5, 2015, Boston, Massachusetts, United States

DETC2015-46861

DECOMPOSITION-BASED DESIGN OPTIMIZATION OF HYBRID ELECTRIC POWERTRAIN ARCHITECTURES: SIMULTANEOUS CONFIGURATION AND SIZING DESIGN

Alparslan Emrah Bayrak
Mechanical Engineering
University of Michigan
Ann Arbor, Michigan, 48109
Email: bayrak@umich.edu

Namwoo Kang*
Mechanical Engineering
University of Michigan
Ann Arbor, Michigan, 48109
Email: nwkang@umich.edu

Panos Y. Papalambros
Mechanical Engineering
University of Michigan
Ann Arbor, Michigan, 48109
Email: pyp@umich.edu

ABSTRACT

Effective electrification of automotive vehicles requires designing the powertrain's configuration along with sizing its components for a particular vehicle type. Employing planetary gear systems in hybrid electric vehicle powertrain architectures allows various architecture alternatives to be explored, including single-mode architectures that are based on a fixed configuration and multi-mode architectures that allow switching power flow configuration during vehicle operation. Previous studies have addressed the configuration and sizing problems separately. However, the two problems are coupled and must be optimized together to achieve system optimality. An all-in-one system solution approach to the combined problem is not viable due to the high complexity of the resulting optimization problem. In this paper we propose a partitioning and coordination strategy based on Analytical Target Cascading for simultaneous design of powertrain configuration and sizing for given vehicle applications. The capability of the proposed design framework is demonstrated by designing powertrains with one and two planetary gears for a mid-size passenger vehicle.

1 Introduction

Effective electrification of automotive powertrains requires solving the coupled topology and sizing design problem. Evaluation of design performance further depends on the control (or power management) strategy that distributes the power demand to the engine and motor/generators. Hybrid Electric Vehicle (HEV) powetrain design is thus a challenging coupled design (topology and size) and control problem. To complicate matters further, an HEV *configuration* is a connection scheme among powertrain components and the vehicle's output shaft(s), and some designs allow changing the configuration during vehicle operation using mechanical clutches. Each of these particular configurations is called the *driving mode* or simply *mode*. We define the collection of these modes (i.e., configurations) as the HEV *architecture*. The so-called power-split designs that can have a single-mode (see Figure 2) or multi-mode architecture (see Figure 3) connect the powertrain components to the vehicle output shaft in different ways using Planetary Gear (PG) systems depending on the vehicle operational requirements. Existing architectures include 1-PG [1, 2], 2-PG [3–7], and 3-PG [8, 9] architectures. In the remainder, we use the terms configuration, architecture and mode as defined above and avoid using the term topology.

Previous HEV powertrain design research has focused on designing architecture for a given application and fixed powertrain component sizes and gear ratios. [10–13]. Since feasible configurations define a disjoint design space, an all-in-one strategy cannot be used to to solve the combined architecture and sizing problem. This paper formulates the combined optimal architecture, sizing, and control problem and employs a decomposition-based optimization strategy, Analytical Target

*Address all correspondence to this author.

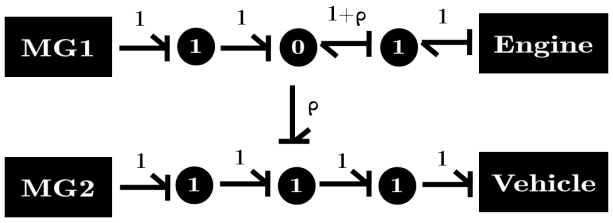

FIGURE 1. Modified bond graph representation of the Toyota Prius architecture where ρ is the ring to sun planetary gear ratio.

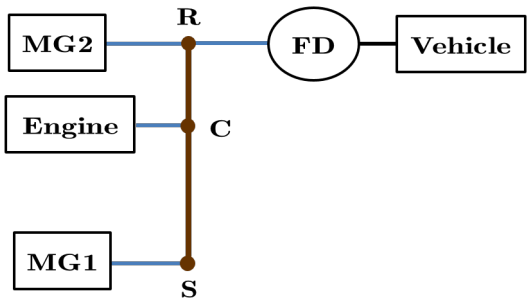

FIGURE 2. Lever representation of the Toyota Prius architecture. "R", "C" and "S" denote the ring, carrier and sun gears, respectively. "FD" denotes the final drive.

Cascading (ATC), to solve it. ATC is a hierarchical optimization methodology for multilevel systems developed by [14, 15] with proven convergence under certain assumptions [15] and demonstrated in industrial applications (e.g., [16, 17]) Further generalization and computational improvement of ATC can be achieved using Augmented Lagrangian relaxation [18, 19]. A Battery-HEV (BHEV) without plug-in capability will be used as a demonstration example.

The organization of the rest of the paper is as follows: Section 2 summarizes how architecture alternatives are created. Section 3 describes the formulation of the general HEV architecture optimization problem that combines configurations, sizing and control using ATC. Section 4 presents results and discussion for the demonstration example and Section 5 offers conclusions.

2 HEV Architecture Representation and Generation

We classify power-split architectures as single-mode, based on a fixed configuration, and multi-mode, consisting of multiple configurations. In this section we describe a representation model for single- and multi-mode architectures and summarize the process to generate feasible powertrain configurations.

The "modified bond graph" model described in [12] is chosen to represent architecture decisions. Figure 1 shows the modified bond graph model corresponding to a Toyota Prius- architecture shown in the lever analogy [20] of Figure 2. Vehicle output and powertrain components such as engine and motor/generators (MGs) appear in every possible design candidate, so they are not design decisions and are represented by fixed "boxes." Connections among components through PGs are represented by bonds connected at "0" and "1" junctions. Each bond has its associated causal stroke and a bond weight (1, ρ or $1+\rho$ where ρ is the PG ratio) that corresponds to a transformer modulus in the conventional bond graph representation. Using the modified bond graph representation we generate all feasible configuration alternatives for single- and multi-mode architectures.

2.1 Single-mode architecture

The single-mode architecture in Figure 2 consists of a fixed configuration represented by a single modified bond graph, Figure 1. In the BHEV example we use, there is no external charge source and so the architecture must sustain the battery state of charge throughout the drive cycle, i.e, pure electric configurations without an engine are not considered feasible.

A 2×2 kinematic matrix denoted by $\mathbf{C}_{mode}$ is extracted from the modified bond graph representation to analyze the architecture. We define $\mathbf{C}_{mode}$ as:

$$\mathbf{C}_{mode} \begin{bmatrix} \omega_{eng} \\ \omega_{out} \end{bmatrix} = \begin{bmatrix} \omega_{MG1} \\ \omega_{MG2} \end{bmatrix}, \tag{1}$$

where $\omega_{eng}, \omega_{out}, \omega_{MG1}$ and ω_{MG2} denote the rotational speeds of the engine, output shaft, MG1 and MG2, respectively. Using the input and output power equality, the torque relationships can be derived:

$$-\mathbf{C}_{mode}^{-T} \begin{bmatrix} T_{eng} \\ -T_{out} \end{bmatrix} = \begin{bmatrix} T_{MG1} \\ T_{MG2} \end{bmatrix}. \tag{2}$$

2.2 Multi-mode architecture

A modified version of the Chevrolet Volt architecture shown in Figure 3 is an example of a multi-mode architecture. The Chevrolet Volt architecture has four modes with three clutches but here we remove the series hybrid mode and show only three modes so we can focus on only power-split architectures. Pure-electric configurations are feasible for multi-mode architectures as long as a hybrid mode exists. In Figure 3, when only Clutch (CL) 2 is engaged, a hybrid mode is obtained. When both CL1 and CL2 are engaged, the engine is connected to the ground and a pure electric mode is generated. When none of the clutches are engaged, the engine is disconnected from the architecture and another pure electric mode is generated.

We represent each of these particular configurations with a separate modified bond graph. Combining all three graphs represents the multi-mode architecture. An additional step is to calculate the number of clutches needed to combine the configurations. We use the number of clutches in the architecture as

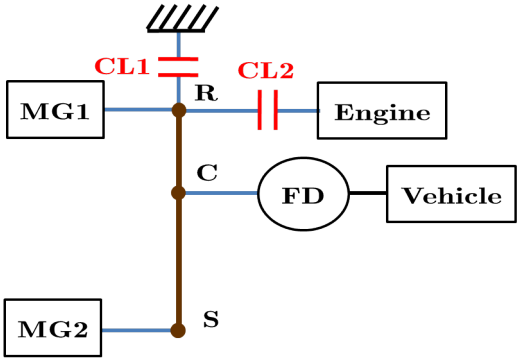

FIGURE 3. Lever representation of three modes of the Chevrolet Volt architecture. (Series hybrid mode removed)

a complexity measure and use this measure to limit acceptable complexity in the generated architectures. As described in [13] the number of clutches needed can be calculated by comparing the modified bond graphs. Hybrid modes in multi-mode architectures can be analyzed in the same way as described in Section 2.1. The first pure-electric mode in Figure 3 is a 1-degree-of-freedom (dof) configuration whose 2×2 kinematic matrix can be defined as follows:

$$\begin{bmatrix} 1 \\ 0 \end{bmatrix} \omega_{out} = \mathbf{C}_{mode} \begin{bmatrix} \omega_{MG1} \\ \omega_{MG2} \end{bmatrix}. \tag{3}$$

The second pure electric mode is a 2-dof configuration and we define its 1×2 kinematic matrix as:

$$\omega_{out} = \mathbf{C}_{mode} \begin{bmatrix} \omega_{MG1} \\ \omega_{MG2} \end{bmatrix}. \tag{4}$$

When evaluating performance or fuel consumption of a multi-mode architecture, we shift the kinematic matrices when the mode is shifted.

2.3 Architecture generation

The generation process has four main steps: (i) Given all powertrain components and number of PGs, the number of internal and external junctions are determined, and all possible simple and connected, undirected graphs are enumerated; (ii) for each undirected graph, junction types are assigned to the nodes and causal strokes obeying bond graph rules are assigned to the edges; (iii) bond weights representing the kinematic relationships among the gears of PG sets are assigned to the bonds; (iv) kinematic matrices described in Sections 2.1 and 2.2 are extracted from the modified bond graphs for the analysis of the configurations. Details of the feasible configuration generation process are described in [12]. Only a brief summary of the results is presented here.

Using two MGs, one output shaft, one (optional) engine and one (optional) ground, we generate 52 distinct feasible configurations for one PG, with 16 being hybrid and 36 being pure electric. Using the same set of powertrain components with two PGs, we generate 3420 feasible configurations with 2124 being hybrid and 1296 being pure electric. Some of these distinct 2-PG configurations may have the same kinematic matrix. For instance, when both PG ratios are equal to 2, the 2124 hybrid configurations result in 1178 unique $\mathbf{C}_{mode}$ matrices. These kinematically equivalent designs can be useful for multi-mode designs, for example, with two kinematically equivalent configurations we may select one with fewer clutches.

3 Generalized architecture design

The generalized architecture design problem involves selecting optimal powertrain configurations along with component sizes and control strategy that minimize fuel consumption and satisfy performance constraints. We present the mathematical formulation of the combined problem and describe a solution strategy.

3.1 Problem formulation

The mathematical formulation of the generalized architecture design problem is:

General HEV Architecture Design Problem

$$\begin{aligned}
&\text{min} \quad f_{cons}(\mathbf{x}_c(N_{mode}), \mathbf{x}_s, \psi(t, \mathbf{x}_c(N_{mode}), \mathbf{x}_s, \mathbf{p})) \\
&\text{with respect to (w.r.t)} \\
&\qquad \{\mathbf{x}_c(N_{mode}),\ \mathbf{x}_s,\ \psi(t, \mathbf{x}_c(N_{mode}), \mathbf{x}_s, \mathbf{p})\} \\
&\text{subject to (s.t.)} \\
&\qquad \mathbf{g}_{perf}(\mathbf{x}_c(N_{mode}), \mathbf{x}_s, \psi(t, \mathbf{x}_c(N_{mode}), \mathbf{x}_s, \mathbf{p})) \leq \mathbf{0} \\
&\qquad g_{complex}(\mathbf{x}_c(N_{mode})) \leq \mathbf{0} \\
&\qquad \psi(t, \mathbf{x}_c(N_{mode}), \mathbf{x}_s, \mathbf{p}) \text{ is attainable} \\
&\qquad lb \leq \mathbf{x}_s \leq ub \\
&\qquad N_{mode} \in \{1, 2, 3, 4, ...\} \\
&\qquad \mathbf{x}_c \text{ is feasible.}
\end{aligned} \tag{5}$$

The objective to minimize f_{cons} is the fuel consumption of the vehicle under a given set of drive cycles defined over time t. The objective depends on the configuration represented by a vector $\mathbf{x}_c$, the size of the powertrain components including gear ratios $\mathbf{x}_s$ (design variables), the supervisory control policy ψ that distributes the demanded power to engine and MGs (control variable), and vehicle parameters $\mathbf{p}$ such as vehicle mass, wheel inertia, vehicle frontal area, and aerodynamic drag. Here we focus on the case where $\mathbf{x}_s$ includes only the PG ratios and final drive ratio. Models for the engine, MGs and battery with respect to their sizing variables can also be included in a more general case. The size of the vector $\mathbf{x}_c$ depends on the number of modes in the architecture denoted by N_{mode}.

The first set of constraints $\mathbf{g}_{perf}$ describes the performance requirements for the architecture including 0 to 60 Miles Per Hour (MPH) acceleration time, top speed or gradeability. The next constraint denoted by $g_{complex}$ is the complexity constraint measured by the number of clutches in the architecture as discussed in Section 2.2. The sizing variables are bounded by upper and lower bounds denoted by ub and lb, respectively. The control policy ψ must be attainable within the limits of the components and $\mathbf{x}_c$ must correspond to a feasible configuration.

3.2 Combined design and control problem

Solution strategies for the combined design and control problem can be classified as *sequential*, *iterative*, *simultaneous* and *nested* [21,22]. The sequential strategy assumes that the design and control problems are fully separable and does not necessarily find the system optimum since it lacks the coupling term. The iterative strategy solves the design and control problems multiple times in sequence until convergence, although convergence to the system optimum is not guaranteed. The simultaneous strategy is an All-In-One (AIO) formulation, and the nested strategy solves the control problem at each (external) design iteration. Both latter strategies can achieve system optimality. The nested strategy is used here for simplicity.

Solving the control problem within the nested strategy can be achieved with Dynamic Programming (DP) [23, 24], Pontryagin's Minimum Principle (PMP) [25, 26] and Equivalent Consumption Minimization Strategy (ECMS) [27]. As discussed in [26, 28], ECMS is not an optimal control strategy for general problems, but it can provide results close to the PMP with some simplified battery assumptions. Here we use ECMS for its computational efficiency. ECMS implementation details are described in [12].

3.3 Problem solution via decomposition

If $\mathbf{x}_c$ is represented by a modified bond graph, i.e., a vector consisting of adjacency matrix, junction types, causalities and weights on each bond, one approach is to define the elements of $\mathbf{x}_c$ as integer variables and $\mathbf{x}_s$ as continuous, and solve the AIO problem using a derivative-free algorithm. However, not every modified bond graph corresponds to a feasible configuration. The feasibility constraints on $\mathbf{x}_c$ define a very small and disjoint design space, and derivative-free methods do not work. We can enumerate all feasible configurations to create a feasible design space for $\mathbf{x}_c$ and optimize $\mathbf{x}_s$ for each feasible configuration. The nested control problem is computationally expensive, and so enumeration can work for a small number of feasible configurations such as for 1-PG single-mode architectures with 16 feasible configurations.

An alternative representation uses continuous variables for both configuration and sizing. The kinematic relationship matrix $\mathbf{C}_{mode}$ introduced in Section 2 depends on both configuration and PG ratios. To include the final drive ratio we define:

$$\mathbf{C}_{conf}(\mathbf{x}_c, \mathbf{x}_s) = \begin{cases} \mathbf{C}_{mode} \cdot \begin{bmatrix} 1 & 0 \\ 0 & FR \end{bmatrix} & if \text{ hybrid mode} \\ \mathbf{C}_{mode} \cdot 1/FR & if \text{ pure electric mode,} \end{cases} \tag{6}$$

where $\mathbf{x}_s = \begin{bmatrix} \boldsymbol{\rho} \\ FR \end{bmatrix}$, $\boldsymbol{\rho}$ is the vector of PG ratios and FR is the final drive ratio. The elements of $\mathbf{C}_{conf}$ can be optimized to minimize fuel consumption with vehicle performance constraints as proposed by Cheong et al. [29]. However, contrary to the case discussed by Cheong et al., not all $\mathbf{C}_{conf}$ matrices correspond to feasible configurations. For example, Figure 4 shows the projections of 4-dimensional feasible design space of $\mathbf{C}_{conf}$ elements onto 2-dimensional planes for 1-PG hybrid modes. The empty regions in the design space correspond to infeasible configurations.

Defining constraints for $\mathbf{C}_{conf}$ feasibility becomes complicated as the number of PGs increases. For a general formulation accounting for feasibility we introduce partitions for single-mode and multi-mode design subproblems and use ATC to coordinate them. The general ATC subproblem P_{ij} corresponding to the j-th element at the i-th level is:

$$\begin{aligned} \min \quad & f_{ij}(\bar{\mathbf{x}}_{ij}) + \phi(\mathbf{c}) \\ \text{w.r.t.} \quad & \bar{\mathbf{x}}_{ij} = [\mathbf{x}_{ij}, \mathbf{t}_{(i+1)k_1}, \ldots, \mathbf{t}_{(i+1)k_{n_{c_{ij}}}}] \\ \text{s.t.} \quad & \mathbf{g}_{ij}(\bar{\mathbf{x}}_{ij}) \leq \mathbf{0} \\ & \mathbf{h}_{ij}(\bar{\mathbf{x}}_{ij}) = \mathbf{0} \\ \text{where } & \mathbf{c} = [(\mathbf{t}_{ij} - \mathbf{r}_{ij}), (\mathbf{t}_{(i+1)k_1} - \mathbf{r}_{(i+1)k_1}), \ldots, \\ & \qquad (\mathbf{t}_{(i+1)k_{n_{c_{ij}}}} - \mathbf{r}_{(i+1)k_{n_{c_{ij}}}})] \\ & \phi(\mathbf{c}) = \mathbf{v}^T(\mathbf{c}) + \|\mathbf{w} \circ \mathbf{c}\|_2^2 \ . \end{aligned} \tag{7}$$

Here, f_{ij} is the local objective function, $\bar{\mathbf{x}}_{ij}$ is the vector of optimization variables, $\mathbf{x}_{ij}$ is the vector of local design variables, $\mathbf{g}_{ij}$ and $\mathbf{h}_{ij}$ are the local inequality and equality constraints, respectively, $\mathbf{t}_{ij}$ is the vector of children target optimization variables, $\mathbf{r}_{ij}$ is the vector of local element responses, $n_{c_{ij}}$ is the number of children, $\mathbf{c}$ is the vector of inconsistencies between targets and responses, and ϕ is a penalty function.

The augmented Lagrangian penalty function formulation with alternating direction method of multipliers [19] is used, where $\mathbf{v}$ is the vector of Lagrange multipliers, $\mathbf{w}$ is the vector of quadratic penalty weights, and the Hadamard symbol $\circ$ is used to denote term-by-term multiplication of vectors. After solving all subproblems of iteration k, the penalty weights are updated according to

$$\mathbf{w}^{k+1} = \beta \mathbf{w}^k, \tag{8}$$

where $\beta \geq 1$ (to speed up convergence, it is recommended that $2 < \beta < 3$). The Lagrange multiplier estimates are updated

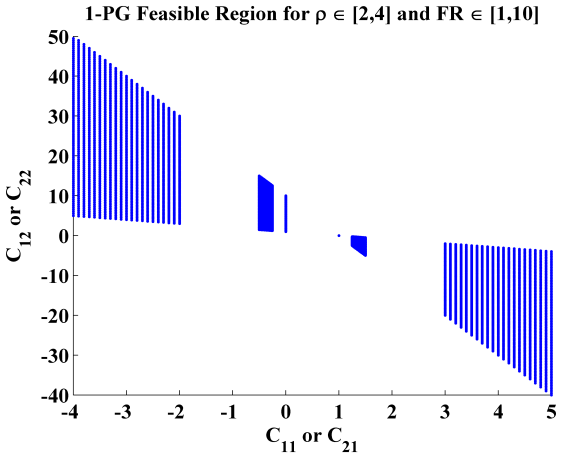

(a) C_{11} vs C_{12} (or C_{21} vs $C22$)

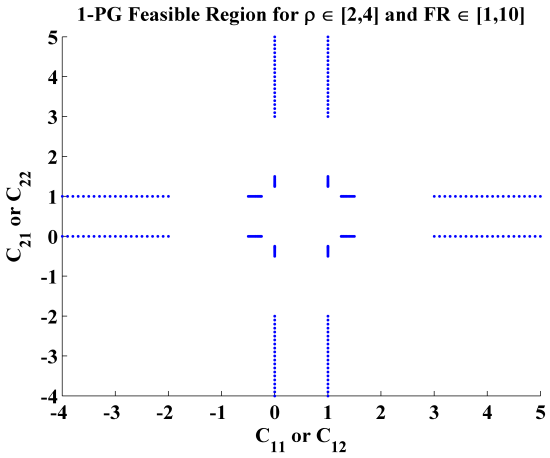

(b) C_{11} vs C_{21} (or C_{12} vs $C22$)

FIGURE 4. Projection of the 4D feasible region of $\mathbf{C}_{conf}$ for 1-PG hybrid designs to 2D planes

according to

$$\mathbf{v}^{k+1} = \mathbf{v}^k + 2\ \mathbf{w}^k \circ \mathbf{w}^k \circ \mathbf{c}^k. \tag{9}$$

Two termination criteria are used: The change in the maximal consistency constraint value after two consecutive iterations must be smaller than a positive threshold ε_1

$$\|\mathbf{c}^k - \mathbf{c}^{k-1}\|_\infty < \varepsilon_1. \tag{10}$$

and the maximal consistency constraint violation must be smaller than a positive threshold ε_2

$$\|\mathbf{c}^k\|_\infty < \varepsilon_2. \tag{11}$$

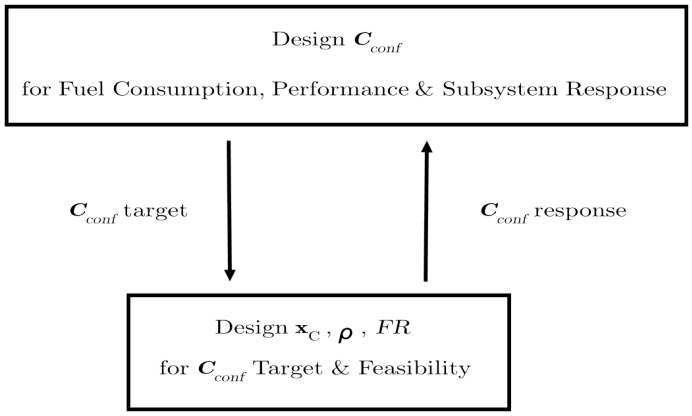

FIGURE 5. Decomposition of combined single-mode architecture and gear ratio design

3.3.1 Single-mode architecture design The problem partitioning for single-mode architecture design is shown in Figure 5. The system level solves the fuel consumption minimization problem with respect to $\mathbf{C}_{conf}$ considering vehicle performance and subsystem response. The system problem does not consider feasibility of $\mathbf{C}_{conf}$. The system-level solution is sent to the subsystem level as a target. The subsystem problem tries to meet this target as close as possible by designing gear ratios for feasible configurations. The system-level problem is formulated as follows:

$$\begin{aligned}
\min\quad & f_{cons}(\mathbf{C}^U_{conf}, \psi^*(t, \mathbf{C}^U_{conf}, \mathbf{p})) + \phi(\mathbf{C}^U_{conf} - \mathbf{C}^L_{conf}) \\
\text{w.r.t.}\quad & [C_{11}, C_{12}, C_{21}, C_{22}], \text{where } \mathbf{C}^U_{conf} = \begin{bmatrix} C_{11} & C_{12} \\ C_{21} & C_{22} \end{bmatrix} \\
\text{s.t.}\quad & \mathbf{g}_{perf}(\mathbf{C}^U_{conf}, \psi^*(t, \mathbf{C}^U_{conf}, \mathbf{p})) \leq \mathbf{0} \\
& lb \leq \mathbf{C}^U_{conf} \leq ub \\
& |det(\mathbf{C}^U_{conf})| > 0
\end{aligned} \tag{12}$$

where ϕ is the augmented Lagrangian penalty function [19]. Superscripts $(\cdot)^U$ and $(\cdot)^L$ indicate upper and lower system variables, respectively. ψ^* denotes the optimal control strategy obtained from a nested formulation. The elements of $\mathbf{C}_{conf}$ are continuous design variables and all invertible $\mathbf{C}_{conf}$ are assumed to be feasible. A two degree-of-freedom hybrid configuration must have a non-singular $\mathbf{C}_{conf}$. So we include invertibility as a constraint at the system level. The optimal $\mathbf{C}_{conf}$ obtained by the system-level problem is passed to the subsystem level as a target. The subsystem problem addresses feasibility of $\mathbf{C}_{conf}$ based on the feasible configurations generated earlier. The sub-

system problem is stated as follows:

$$\begin{aligned} \min \quad & \phi(\mathbf{C}^U_{conf} - \mathbf{C}^L_{conf}) \\ \text{w.r.t.} \quad & \mathbf{x} = [\mathbf{x}_c, \mathbf{x}_s]^T, \text{ where } \mathbf{x}_s = [\boldsymbol{\rho}, FR]^T \\ \text{s.t.} \quad & lb \leq \mathbf{x}_s \leq ub \\ & \mathbf{x}_c \text{ is feasible} \\ \text{where} \quad & \mathbf{C}^L_{conf} = f_{conf}(\mathbf{x}) \end{aligned} \tag{13}$$

where f_{conf} is a function that maps the configuration and gear ratios to the kinematic relationship matrix. We solve this problem with respect to $\mathbf{x}_s$ for all feasible $\mathbf{x}_c$ separately and select the set of $\mathbf{x} = [\mathbf{x}_c, \mathbf{x}_s]^T$ that meet the target the best. Since the subsystem problem does not involve controls, evaluation of f_{conf} is almost instantaneous and computational cost is very low.

3.3.2 Multi-mode architecture design

In the multi-mode architecture design, the main partitioning idea remains the same. However, the system- and subsystem-level formulations slightly differ from the single-mode design. Problem partitioning is depicted in Figure 6. The number of subsystems is equal to the number of modes to be designed. As seen in Figure 6, the sizing variables are shared among subsystems. The design variables of the system-level problem are the elements of $\mathbf{C}_{conf}$ matrix of all the modes in the architecture and sizing variables. The objective of the system-level problem has an additional penalty on the difference between targets and responses for these shared variables. The complexity constraint mentioned earlier appears in each subsystem. The formulation for the system-level problem is:

$$\begin{aligned} \min \quad & f_{cons}(\mathbf{C}^U_{conf,i}, \psi^*(t, \mathbf{C}^U_{conf,i}, \mathbf{p})) \\ & + \sum_{i=1}^{N_{mode}} \phi(\mathbf{C}^U_{conf,i} - \mathbf{C}^L_{conf,i}) + \phi(\mathbf{x}^U_s - \mathbf{x}^L_{s,i}) \\ \text{w.r.t.} \quad & [C_{11,i}, C_{12,i}, C_{21,i}, C_{22,i}, \mathbf{x}^U_s], \\ \text{where} \quad & \mathbf{C}^U_{conf,i} = \begin{bmatrix} C_{11,i} & C_{12,i} \\ C_{21,i} & C_{22,i} \end{bmatrix} \forall i \in \{1, ...N_{mode}\} \\ \text{s.t.} \quad & \mathbf{g}_{perf}(\mathbf{C}^U_{conf,i}, \psi^*(t, \mathbf{C}^U_{conf,i}, \mathbf{p})) \leq \mathbf{0} \\ & lb_i \leq \mathbf{C}^U_{conf,i} \leq ub_i \\ & |det(\mathbf{C}^U_{conf,i})| > 0_i \end{aligned} \tag{14}$$

where the subscript $(\cdot)_{\cdot,i}$ denotes each individual mode in the architecture. Each $\mathbf{C}_{conf,i}$ optimized at the system level is sent as target to the corresponding subsystems. Also the same $\mathbf{x}_s$ is sent to every subsystem as it is the vector of shared variables. The formulation for a subsystem i becomes:

$$\begin{aligned} \min \quad & \phi(\mathbf{C}^U_{conf,i} - \mathbf{C}^L_{conf,i}) + \phi(\mathbf{x}^U_s - \mathbf{x}^L_{s,i}) \\ \text{w.r.t.} \quad & \mathbf{x}_i = [\mathbf{x}_{c,i}, \mathbf{x}^L_{s,i}], \text{ where } \mathbf{x}^L_{s,i} = [\boldsymbol{\rho}_i, FR_i] \\ \text{s.t.} \quad & g_{complex}(\mathbf{x}_{c,i}, \mathbf{x}_{c,j}) \leq 0 \quad \forall j \in \{1, ...N_{mode} | j \neq i\} \\ & lb_i \leq \mathbf{x}^L_{s,i} \leq ub_i \\ & \mathbf{x}_{c,i} \text{ is feasible} \\ \text{where} \quad & \mathbf{C}^L_{conf,i} = f_{conf}(\mathbf{x}_i) \end{aligned} \tag{15}$$

4 Results and discussion

Key specifications for the vehicle and powertrain components used in the BHEV example are in Table 1.

TABLE 1. Vehicle specifications used for the case studies

Specification	Value
Vehicle Body Mass	$1400[kg]$
Tire Radius	$0.3[m]$
Aerodynamic Drag Coefficient	0.29
Frontal Area	$2[m^2]$
Battery Voltage	$350[V]$
Battery Efficiency	$92[\%]$
Battery Capacity	$6.5[Ah]$
Rated MG1 Power	$42[kW]$
Rated MG2 Power	$60[kW]$
Max MG Speed	12000 [rpm]
Max MG Torque	200 [Nm]
Rated Engine Power	$43[kW]$
Max Engine Torque	$102[Nm]$
Engine Displacement Size	$1.5[L]$

Fuel economy f_{mpg} is calculated using the average of city (UDDS) and highway (HWFET) cycle consumptions. The control problem is solved with nested strategy and ECMS as described in Section 3.2. Acceleration time t_{60mph} must be less than 12 sec, and top speed V_{top} at least 105 mph. PG ratios vary between 2 and 4 and final drive ratio between 1 and 10.

ATC allows using different optimizers for each subproblem. We use Genetic Algorithm (GA) for the system-level and Sequential Quadratic Programming (SQP) for the subsystem-level problems. When the problem is partitioned as described in Section 3.3, tests showed that the system level-problem is highly dependent on the initial population selection due to the disjoint nature of the design space. Thus we generate some feasible designs from each configuration and randomly select among them to provide an initial population to the GA. The subsystem-level problem can be expressed analytically by extracting the $\mathbf{C}_{conf}$ ma-

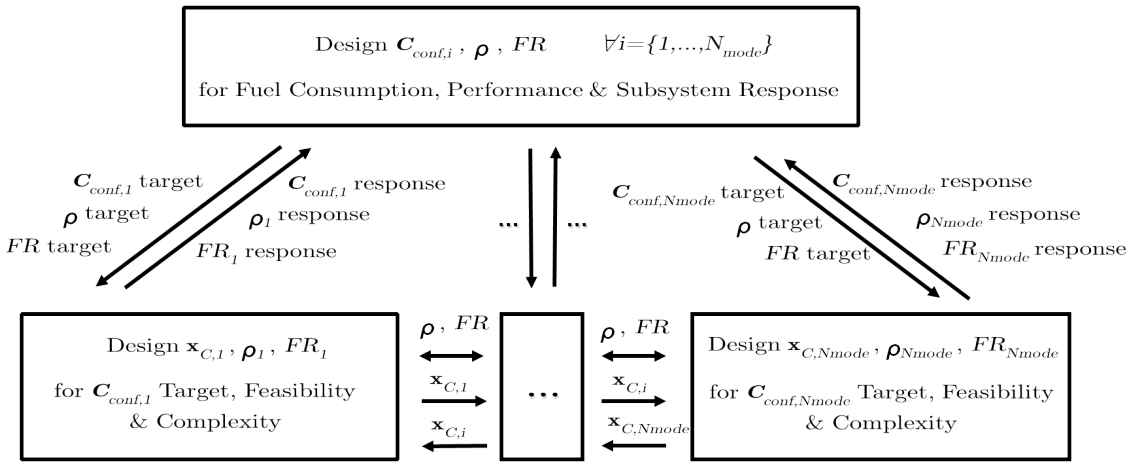

FIGURE 6. Decomposition of combined multi-mode architecture and gear ratio design

trices from the modified bond graph representation and quickly solved with SQP. We use $\varepsilon_1 = \varepsilon_2 = 0.01$ for all problems. We set $\beta = 1.25$ for the results in Sections 4.1, 4.2 and 4.3, ans set $\beta = 1.75$ for the results in Section 4.4.

4.1 Singe-mode 1-PG architecture results

Before implementing the ATC process, we first optimize all 16 configurations using SQP and starting from different initial gear ratio selections, and select the best one. See Table 2. We take these optimal results as a reference point when evaluating ATC solutions.

TABLE 2. Single-mode 1-PG architecture design results for optimizing each configuration separately

Initial $\begin{bmatrix}\rho_0\\FR_0\end{bmatrix}$	Optimal $\begin{bmatrix}\rho^*\\FR^*\end{bmatrix}$	Optimal $\mathbf{C}_{conf}$	f_{mpg} [mpg]	V_{top} [mph]	t_{60mph} [sec]
$\begin{bmatrix}2\\1.5\end{bmatrix}$	$\begin{bmatrix}2.01\\4.27\end{bmatrix}$	$\begin{bmatrix}3.01 & -8.59\\0 & 4.27\end{bmatrix}$	56.81	108	11.66
$\begin{bmatrix}2.5\\2.5\end{bmatrix}$	$\begin{bmatrix}2.00\\4.25\end{bmatrix}$	$\begin{bmatrix}3.00 & -8.50\\0 & 4.29\end{bmatrix}$	56.80	108	11.74
$\begin{bmatrix}3\\3.5\end{bmatrix}$	$\begin{bmatrix}2.00\\4.29\end{bmatrix}$	$\begin{bmatrix}3.00 & -8.57\\0 & 4.29\end{bmatrix}$	56.87	108	11.64

The results in Table 2 are close. Some hit the PG ratio lower bound. Relaxing the bound is limited by PG design practicality. The smallest pinion gear size limits the PG ratio to 2 in practice [30]. The architecture corresponding to these results is the same as the 1-PG architecture of the Toyota Prius shown in Figure 2.

When solving the problem given in Section 3.3.1 for 1-PG configurations, we provide feasible initial populations selected randomly from the pool of feasible designs generated from each configuration for the system-level problem. In order to ensure variety, we select designs from each feasible configuration. We set the population size to 100 and select three sets of populations. The ATC process converges after 11, 21 and 8 iterations for each of the three initial populations, respectively. The results are shown in Table 3.

TABLE 3. ATC results for single-mode 1-PG architecture design using GA with 5 generations for the system level problem

Optimal $\mathbf{C}_{conf}$	Optimal $\mathbf{x}_s$	f_{mpg} [mpg]	V_{top} [mph]	t_{60mph} [sec]
$\begin{bmatrix}3.67 & -11.46\\0 & 4.28\end{bmatrix}$	$\rho^* = 2.67$ $FR^* = 4.28$	56.37	111	10.73
$\begin{bmatrix}3.84 & -12.00\\0 & 4.21\end{bmatrix}$	$\rho^* = 2.85$ $FR^* = 4.21$	56.24	111	11.98
$\begin{bmatrix}4.07 & -11.58\\0 & 3.77\end{bmatrix}$	$\rho^* = 3.07$ $FR^* = 3.77$	56.35	109	11.57

The configurations are all the same as the one in Figure 2. The GA results are consistent and close to the results obtained from optimizing each configuration one by one. Both approaches converge to the same configuration with some difference in the gear ratios. After ATC converges, we can use a local search on the gear ratios using the final configuration to fine-tune the

results. The number of generations necessary depends on the problem. In this case it was empirically set to 5. Increasing the generation number does not show any significant improvement in the results [31].

4.2 Singe-mode 2-PG architecture results

When we increase the number of PGs in the architecture, the system-level problem does not change but the subsystem problem has more design variables and more configurations to search. Due to the complexity of the problem, the exhaustive enumeration used to validate the results of the proposed method in the 1-PG case is not possible in 2-PG case but we can use the lessons learned from the 1-PG study to increase the chance of finding good designs. For example, in the 1-PG case the system-level solution is affected by the initial population selection due to the disjoint feasible space; to reduce this effect we provide a variety of configurations in the initial population. When selecting initial population, we have more than 100 feasible configurations in this case. We can group the designs based on the sign of the elements of $\mathbf{C}_{conf}$ matrix. Since this matrix has four elements and each element can be either positive, negative or zero, we have 81 possible types of $\mathbf{C}_{conf}$ matrices. Selecting randomly 100 designs in total from each of these groups, we tested three initial populations. ATC converged after 4, 3 and 3 iterations for the three initial populations, respectively. Table 4 shows the results for this case.

TABLE 4. ATC results for single-mode 2-PG architecture design using GA with 5 generations for the system level problem

Optimal $\mathbf{C}_{conf}$	Optimal $\mathbf{x}_s$	f_{mpg} [mpg]	V_{top} [mph]	t_{60mph} [sec]
$\begin{bmatrix} 4.33 & -11.48 \\ 0 & 4.62 \end{bmatrix}$	$\rho_1^* = 3.33$ $\rho_2^* = 2.94$ $FR^* = 3.44$	57.56	105	11.44
$\begin{bmatrix} 4.56 & -11.94 \\ 0 & 4.5 \end{bmatrix}$	$\rho_1^* = 3.55$ $\rho_2^* = 2.94$ $FR^* = 3.35$	57.51	105	11.52
$\begin{bmatrix} 3.98 & -11.28 \\ 0 & 5.33 \end{bmatrix}$	$\rho_1^* = 2.45$ $\rho_2^* = 2.98$ $FR^* = 3.78$	57.81	105	10.65

The computations consistently converged to similar optimal designs and the configuration corresponding to these $\mathbf{C}_{conf}$ is in Figure 7.

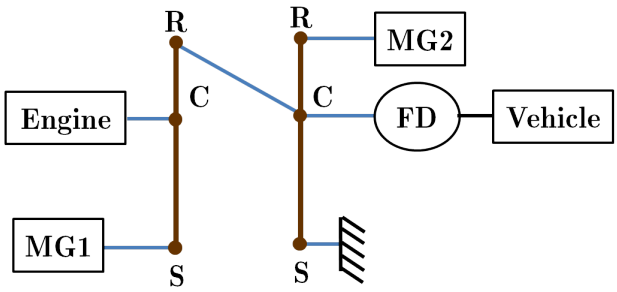

FIGURE 7. Optimal single-mode 2-PG architecture obtained by ATC

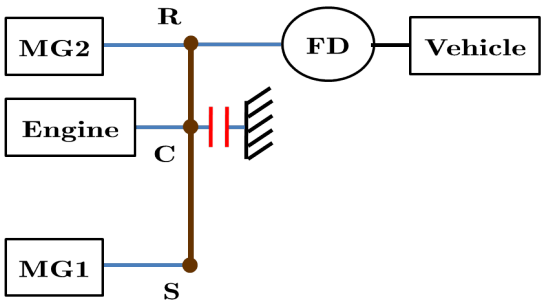

FIGURE 8. Optimal 1-PG dual-mode obtained by ATC

TABLE 5. ATC results for dual-mode 1-PG architecture design using GA with 5 generations for the system level problem

Optimal $\mathbf{C}_{conf,1}$	Optimal $\mathbf{C}_{conf,2}$	Optimal $\mathbf{x}_s$	f_{mpg} [mpg]	V_{top} [mph]	t_{60mph} [sec]
$\begin{bmatrix} 3.00 & -9.37 \\ 0 & 4.68 \end{bmatrix}$	$\begin{bmatrix} 0 & -0.21 \\ 0.21 & 0.43 \end{bmatrix}$	$\rho^* = 2.00$ $FR^* = 4.68$	58.46	110	7.09
$\begin{bmatrix} 3.08 & -10.25 \\ 0 & 4.92 \end{bmatrix}$	$\begin{bmatrix} 0 & -0.20 \\ 0.20 & 0.41 \end{bmatrix}$	$\rho^* = 2.08$ $FR^* = 4.93$	59.97	112	7.04
$\begin{bmatrix} 3.03 & -9.60 \\ 0 & 4.72 \end{bmatrix}$	$\begin{bmatrix} 0 & -0.21 \\ 0.21 & 0.43 \end{bmatrix}$	$\rho^* = 2.03$ $FR^* = 4.72$	58.83	111	7.11

4.3 Dual-mode 1-PG architecture results

We solve the multi-mode architecture design problem formulated in Section 3.3.2 for two modes using 1-PG configurations with the same settings as before. ATC converged after 27, 9 and 25 iterations for the three initial population, respectively. See Table 5. Three initial populations with similar optimal results converged to the dual-mode architecture depicted in Figure 8.

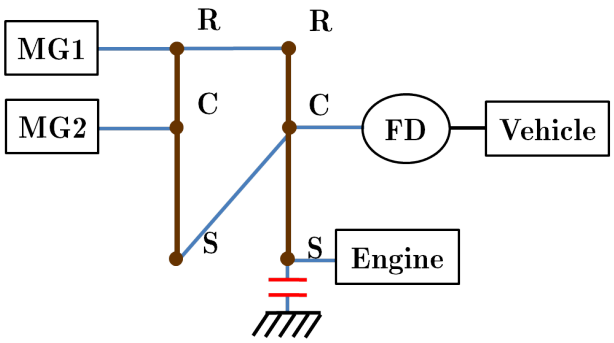

FIGURE 9. Optimal 1-PG dual-mode obtained by ATC

4.4 Multi-mode 2-PG architecture results

We solve the multi-mode architecture design problem for two modes using 2-PG configurations. Since the number of possible architectures is much larger compared to the previous cases, we increase the number of initial population to 300 in order to provide more variety. ATC converged after 12, 12 and 27 iterations for the three initial population, respectively. See Table 5. In this case, two of the optimization runs converged to the same architecture but the last results converged to an infeasible design with a different architecture violating 0-60 mph acceleration time constraint. The violated constraint is highlighted in bold. The optimal architecture obtained in the first two optimization runs is shown in Figure 9. These results show that this case is more sensitive to the initial population selection. Considering the number of possible architecture candidates for this case, it is expected outcome. The dependency of the results on the initial population can be reduced by increasing the initial population size and generation number further. That way more reliable results and possibly better architectures can be obtained in the design process.

5 Conclusion and Future Work

We proposed a formulation and a partitioning and coordination strategy based on ATC to address the combined optimal HEV architecture, sizing, and control problem. We solved the system-level problem using a specially-seeded GA and the subsystem-level problems using SQP. We demonstrated the framework with a BHEV example for a mid-size passenger vehicle. Different initial populations consistently converged to the same architecture with some variations in the gear ratios in each case.

The variation in the optimal gear ratios from the optimization runs with different initial populations can be eliminated by performing an additional local search on the gear ratios after ATC converges. As shown in Table 2 optimizing only the gear ratios gives consistently similar optimal results. However, optimizing the gear ratios for all feasible configurations would not be tractable for a problem with too many feasible configurations. Therefore, having an optimal configuration from ATC can be used as a good initial guess for an additional local search to improve results further. The formulation is general enough to include size variables for other components such as engine, MG, and battery. Adding these variables will increase computational complexity but also the range of decisions that can be included in the architecture system optimization problem.

TABLE 6. ATC results for dual-mode 2-PG architecture design using GA with 5 generations for the system level problem

Optimal $\mathbf{C}_{conf,1}$	Optimal $\mathbf{C}_{conf,2}$	Optimal $\mathbf{x}_s$	f_{mpg} [mpg]	V_{top} [mph]	t_{60mph} [sec]
$\begin{bmatrix} -0.50 & 5.63 \\ -0.34 & 5.04 \end{bmatrix}$	$\begin{bmatrix} 0 & -0.20 \\ 0.26 & -0.30 \end{bmatrix}$	$\rho_1^* = 2.17$ $\rho_2^* = 2.00$ $FR^* = 3.75$	75.22	108	7.12
$\begin{bmatrix} -0.60 & 5.91 \\ -0.40 & 5.16 \end{bmatrix}$	$\begin{bmatrix} 0 & -0.18 \\ 0.27 & -0.31 \end{bmatrix}$	$\rho_1^* = 2.48$ $\rho_2^* = 2.00$ $FR^* = 3.68$	73.79	106	6.87
$\begin{bmatrix} -2.79 & 6.77 \\ 7.40 & -11.44 \end{bmatrix}$	$\begin{bmatrix} 0 & 0.09 \\ 0.56 & 0.33 \end{bmatrix}$	$\rho_1^* = 2.65$ $\rho_{2*} = 2.79$ $FR^* = 1.78$	56.38	117	**27.81**

Acknowledgement

This research has been partially supported by General Motors Corp., the Automotive Research Center, a US Army Center of Excellence at the University of Michigan, and a University of Michigan Graham Sustainability Institute Fellowship. This support is gracefully acknowledged.

REFERENCES

[1] Conlon, B. M., Savagian, P. J., Holmes, A. G., Harpster, M. O., et al., 2011. Output split electrically-variable transmission with electric propulsion using one or two motors, Jan. 11. US Patent 7,867,124.

[2] Sasaki, S., 1998. "Toyota's newly developed hybrid powertrain". In Power Semiconductor Devices and ICs, 1998. ISPSD 98. Proceedings of the 10th International Symposium on, IEEE Press, pp. 17–22.

[3] Schmidt, M., 1996. Two-mode, input-split, parallel, hybrid transmission, Sept. 24. US Patent 5,558,588.

[4] Schmidt, M., 1996. Two-mode, split power, electromechanical transmission, Nov. 26. US Patent 5,577,973.

[5] Holmes, A., Klemen, D., and Schmidt, M., 2003. Electrically variable transmission with selective input split, compound split, neutral and reverse modes, Mar. 4. US Patent 6,527,658.

[6] Holmes, A., and Schmidt, M., 2002. Hybrid electric powertrain including a two-mode electrically variable transmission, Nov. 12. US Patent 6,478,705.

[7] Ai, X., and Anderson, S., 2005. "An electro-mechanical infinitely variable transmisson for hybrid electric vehicles". *SAE Technical Paper 2005-01-0281*.

[8] Schmidt, M., 1999. Two-mode, compound-split electromechanical vehicular transmission, Aug. 3. US Patent 5,931,757.

[9] Raghavan, M., Bucknor, N. K., and Hendrickson, J. D., 2007. Electrically variable transmission having three interconnected planetary gear sets, two clutches and two brakes, Feb. 20. US Patent 7,179,187.

[10] Liu, J., and Peng, H., 2010. "A systematic design approach for two planetary gear split hybrid vehicles". *Vehicle System Dynamics,* ***48***(11), pp. 1395–1412.

[11] Zhang, X., Li, C.-T., Kum, D., and Peng, H., 2012. "Prius+ and volt- : Configuration analysis of power-split hybrid vehicles with a single planetary gear". *IEEE Transactions on Vehicular Technology,* ***61***(8), pp. 3544–3552.

[12] Bayrak, A. E., Ren, Y., and Papalambros, P. Y., 2013. "Design of hybrid-electric vehicle architecture using autogeneration of feasible driving modes". In Proceedings of the ASME 2013 International Design Engineering Technical Conferences, ASME.

[13] Bayrak, A. E., Ren, Y., and Papalambros, P. Y., 2014. "Optimal dual-mode hybrid electric vehicle powertrain architecture design for a variety of loading scenarios". In Proceedings of the ASME 2014 International Design Engineering Technical Conferences, ASME.

[14] Kim, H. M., 2001. "Target cascading in optimal system design". PhD thesis, The University of Michigan.

[15] Michelena, N., Park, H., and Papalambros, P. Y., 2003. "Convergence properties of analytical target cascading". *AIAA journal,* ***41***(5), pp. 897–905.

[16] Kang, N., Kokkolaras, M., and Papalambros, P. Y., 2014. "Solving multiobjective optimization problems using quasi-separable mdo formulations and analytical target cascading". *Structural and Multidisciplinary Optimization,* ***50***, pp. 849–859.

[17] Kang, N., Kokkolaras, M., and Papalambros, P. Y., 2014. "Optimal design of commercial vehicle systems using analytical target cascading". *Structural and Multidisciplinary Optimization*.

[18] Tosserams, S., Etman, L., Papalambros, P., and Rooda, J., 2005. "Augmented lagrangian relaxation for analytical target cascading". In In 6th World Congress on Structural and Multidisciplinary Optimization, May 30–June 3, Citeseer.

[19] Tosserams, S., Etman, L., Papalambros, P., and Rooda, J., 2006. "An augmented lagrangian relaxation for analytical target cascading using the alternating direction method of multipliers". *Structural and Multidisciplinary Optimization,* ***31***(3), pp. 176–189.

[20] Benford, H. L., and Leising, M. B., 1981. The lever analogy: A new tool in transmission analysis. Tech. rep., SAE Technical Paper.

[21] Fathy, H. K., Reyer, J. A., Papalambros, P. Y., and Ulsoy, A. G., 2001. "On the coupling between the plant and controller optimization problems". In American Control Conference, 2001. Proceedings of the 2001, Vol. 3, IEEE Press, pp. 1864–1869.

[22] Peters, D. L., Papalambros, P. Y., and Ulsoy, A. G., 2010. "Relationship between coupling and the controllability grammian in co-design problems". In American Control Conference (ACC), 2010, IEEE Press, pp. 623–628.

[23] Lin, C.-C., Peng, H., Grizzle, J. W., and Kang, J.-M., 2003. "Power management strategy for a parallel hybrid electric truck". *Control Systems Technology, IEEE Transactions on,* ***11***(6), pp. 839–849.

[24] Liu, J., and Peng, H., 2006. "Control optimization for a power-split hybrid vehicle". In American Control Conference, 2006, IEEE Press, pp. 6–pp.

[25] Delprat, S., Guerra, T., and Rimaux, J., 2002. "Control strategies for hybrid vehicles: optimal control". In Vehicular Technology Conference, 2002. Proceedings. VTC 2002-Fall. 2002 IEEE 56th, Vol. 3, IEEE, pp. 1681–1685.

[26] Kim, N., Cha, S., and Peng, H., 2011. "Optimal control of hybrid electric vehicles based on pontryagin's minimum principle". *Control Systems Technology, IEEE Transactions on,* ***19***(5), pp. 1279–1287.

[27] Paganelli, G., Delprat, S., Guerra, T.-M., Rimaux, J., and Santin, J.-J., 2002. "Equivalent consumption minimization strategy for parallel hybrid powertrains". In Vehicular Technology Conference, 2002. VTC Spring 2002. IEEE 55th, Vol. 4, IEEE Press, pp. 2076–2081.

[28] Serrao, L., Onori, S., and Rizzoni, G., 2009. "Ecms as a realization of pontryagin's minimum principle for hev control". In Proceedings of the 2009 conference on American Control Conference, IEEE Press, pp. 3964–3969.

[29] Cheong, K. L., Li, P. Y., and Chase, T. R., 2011. "Optimal design of power-split transmissions for hydraulic hybrid passenger vehicles". In American Control Conference (ACC), 2011, IEEE Press, pp. 3295–3300.

[30] Antony, G. G., and Pantelides, A., 2006. Precision planetary servo gearheads. Tech. rep., American Gear Manufacturers Association.

[31] Bayrak, A. E., 2015. "Topology considerations in hybrid electric vehicle powertrain architecture design". PhD thesis, The University of Michigan.